AIAA JOURNAL
Vol. 39, No. 3, March 2001

Experimental Demonstration of Active Flow Control to Reduce Unsteady Stator–Rotor Interaction

Nikhil M. Rao,* Jinwei Feng,* Ricardo A. Burdisso,† and Wing F. Ng‡
Virginia Polytechnic Institute and State University, Blacksburg, Virginia 24061

An experimental investigation is conducted to reduce the unsteady stator–rotor interaction in a turbofan simulator using active flow control. The fan rotor of a $\frac{1}{14}$-scale turbofan propulsion simulator is subjected to circumferentially periodic inlet flow distortions, generated by four stators that support a centerbody in the inlet mounted onto the simulator. These wakes are reenergized by injecting air from the trailing edge of each stator through discrete blowing holes. The flow rate through each blowing hole is controlled by an individual microelectro-mechanical system based microvalve. The microvalve actuation signal voltage is generated by a proportional–integral–derivative controller and is a function of the wake velocity defect. To determine the successful reenergizing of the wakes, far-field sound pressure level at the blade passing frequency without and with blowing is measured in an anechoic chamber. The active control experiments are performed for two simulator speeds of 29,500 and 40,000 rpm. In addition, the feasibility and advantage of active control is demonstrated by the ability of the system to respond to changes in the inlet flow velocity.

Introduction

LOW-VELOCITY regions or wakes characterize the flowfield downstream of a blade row. These wakes are generated by total pressure losses due to flow over the blades. The passage of these wakes over a downstream stage generates unsteady loading of the downstream blades. On rotor blades, the effect of this unsteady loading generates high sound levels at discrete frequencies and causes blade vibration. The high sound levels are a significant source of environmental noise pollution, and the accumulation of stress cycles due to blade vibration can result in blade failure by high cycle fatigue (HCF). The nature of unsteady interaction is typically dependent on the maximum velocity defect in the wake, the velocity profile across the wake region, the number of defects present, and their spatial periodicity. The velocity profile behind a wake generator is steeper closer to the wake generator and becomes smoother with increasing distance due to mixing. Furthermore, the maximum velocity defect is also higher closer to the wake generator. As noted by Goldstein,[1] these increase the magnitude of unsteady loading on downstream rotor blades. Hence, by increasing the axial spacing between blade rows, the unsteady loading can be reduced. This effect was reported by Pande and Ng,[2] wherein increasing the axial spacing between the stators and fan rotor reduced the far-field noise level of a high-speed turbofan simulator. Trailing-edge blowing (TEB) also aims at reducing the unsteady loading by modifying the wake profile. Reduction or elimination of the velocity defect is achieved by injecting mass from the trailing edge of the wake generator to reenergize the wake. Potential for wake management using TEB to reduce unsteady blade loading has been reported by Waitz et al.[3] Waitz et al. investigated the effect of rotor wake management by removing and or adding fluid from the flow around the rotor blade. Experimentally obtained wake profiles were used in a computational code to predict unsteady loading of the downstream stator and an estimation of the radiated tone was made using LINSUB. This study concluded that wake management is feasible and that TEB is more effective and easier to implement than boundary-layer suction. Naumann,[4] Corcoran,[5] and Park and Cimbala[6] have experimentally shown that TEB reduces significantly both the time-mean wake deficit and unsteadiness in wakes shed by flat plates in a water channel. Naumann[4] showed a reduction of about 90% in the time-mean wake deficit and a reduction of greater than 50% in the turbulent velocity fluctuations. Naumann[4] and Corcoran[5] experimented with various blowing configurations. In particular, Naumann[4] compares a continuous slit and a set of discrete jets, with and without vortex generators. This work showed that the most effective method of TEB was to use a set of discrete jets and that the presence of vortex generators enhanced the mixing of the wake with the jets.

Previous experimental research at Virginia Polytechnic Institute and State University by Leitch,[7] Leitch et al.,[8] and Saunders[9] has demonstrated the effectiveness of TEB in reducing the unsteady stator–rotor interaction. In the work by Leitch[7] and Leitch et al.,[8] different diameters for the TEB holes were used to achieve uniform wake filling along the span of the strut. Hence, optimum wake filling could only be achieved at one particular engine operating condition. In addition, the TEB pressure was adjusted manually. Far-field sound pressure level (SPL) readings showed noise reduction at the blade passing frequency (BPF) tone of up to 7 dB. More recently, Brookfield and Waitz[10] demonstrated on a one-sixth-scale high-bypass-ratio fan stage that TEB of rotating blades was effective for reducing the first three BPF harmonics.

In the present investigation, the TEB scheme developed by Leitch[7] and Leitch et al.[8] is integrated with active control. In this scheme, each blowing hole is supplied individually. Furthermore, all blowing holes have the same diameter. The air supply from a large plenum is directed to each hole using microelectromechanical system (MEMS) based microvalves. The blowing rate of each hole can, if desired, be controlled separately. A signal voltage input from a feedback control algorithm adjusts the flow rate through each microvalve and, hence, the blowing rate of each blowing hole. The active controller generates the signal voltage to drive the minimum wake total pressure to equal the freestream total pressure. This error signal is implemented by using pitot probe flow sensors placed in the wakes and in the free flow. The results show the first reported successful demonstration of active control of TEB from stators in a realistic flow environment. In addition, it is also shown that using active TEB effective wake management is achieved over a range of the simulator operating conditions.

Experimental Setup

Figure 1 shows a schematic of the active control experimental setup used in this research. The components identified are briefly described hereafter.

Received 26 June 1999; revision received 18 February 2000; accepted for publication 28 July 2000.

*Graduate Research Assistant, Vibration and Acoustics Laboratories, Mechanical Engineering Department.

†Professor, Vibration and Acoustics Laboratories, Mechanical Engineering Department.

‡Chris Kraft Professor, Vibration and Acoustics Laboratories, Mechanical Engineering Department. Associate Fellow AIAA.

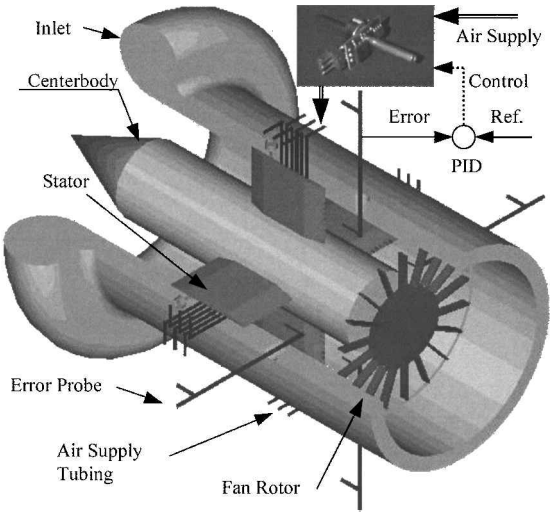

Fig. 1 Experimental setup.

Turbofan Propulsion Simulator

The turbofan propulsion simulator (Model 460) from Tech Development Inc., provides the rotor for investigating stator–rotor unsteady interaction effects. This simulator is modeled on modern, high-bypass-ratio,turbofan engines, and it is represented by the fan rotor in Fig. 1. The simulator has a single-stage axial fan driven by a single-stage axial flow turbine. The fan measures 4.1 in. in diameter and has 18 blades. It is capable of developing a maximum pressure ratio of 1.6, at a mass flow of 2.72 lbm/s, (1.23 kg/s), and maximum speed of 80,000 rpm. The Reynolds number based on the blade tip speed is 1.7×10^6. This value is considerably smaller than for typical flight engines. However, this simulator is used for exploratory research to study the effectiveness of TEB, rather than for an accurate prediction that would require correct flow Reynolds numbers. A row of 26 exit guide vanes (EGVs) is present one rotor chord length downstream of the fan. These guide vanes also cause far-field noise radiation due to the unsteady lift generated by the passage of rotor wakes. The power turbine is a single impulse stage with 29 blades. It is driven by high-pressure air and can handle a maximum mass flow of 1.50 lbm/s, (0.68 kg/s). A magnetic speed pickup mounted in the turbine exhaust cone measures the shaft rotational speed. Thermocouples are provided to monitor the bearing temperatures. Vibration levels are monitored by accelerometers mounted on the inlet. This turbofan simulator is the same one used in previous research on TEB.[7–9]

Inlet

The inlet is a constant area duct with a maximum diameter of 4.1 in. (0.104 m) and a hub diameter of 1.8 in. (0.046 m). The hub is formed by an axisymmetric centerbody with a sharp conical leading edge. Axial grooves are provided in both the centerbody and the inlet to place the stators. The inlet mouth is shaped like a bellmouth to avoid lip separation.

Stator

The unsteady loading of the rotor blades is due to wakes generated by four stators. The primary function of these nonturning stators is to support the centerbody. Figure 2 shows a photograph of the stator. Each stator has a chord of 2.08 in. (0.053 m) and a thickness of 0.25 in. (0.0064 m). The flat faces end in sharp leading and trailing edges. The trailing edge is provided with six blowing holes, with a pitch–hole diameter ratio of two. Each passage is L shaped as shown by the dashed lines in Fig. 2. The passage begins at the top of the stator with a diameter of $\frac{1}{8}$ in. (0.0032 m) and terminates at the trailing edge in a diameter of $\frac{1}{16}$ in. (0.0016 m). A tube connected to the microvalve is inserted into each passage. The stator is held onto the inlet by a bolt, and the air supply tubing protrudes to the outside through a slot cut into the inlet.

MEMS Based Actuator

The flow rate through each blowing hole is controlled by individual MEMS based microvalves, shown in Fig. 1. This individual adjustment of the blowing for each hole should be contrasted with previous research by Leitch[7] and Leitch et al.,[8] where a fixed set of hole diameters were used. The microvalves used for this research are NO-3000 Fluistor™, supplied by Redwood Microsystems. The NO denotes that the microvalves are normally open, that is, if no signal voltage is applied, the microvalves are fully open and operate at maximum flow rate as governed by the source pressure. The design specifications[11] as given by the manufacturer are shown in Table 1. The microvalves operate on the patented thermopneumatic principle. A brief description of the operation, discussed in a private communication with C. F. Lorenzo of NASA Lewis Research Center in 1998 and in Ref. 12, follows. The actuator is a sealed cavity with the control liquid inside it. One wall of the cavity is a diaphragm that flexes when the cavity pressure increases due to evaporation of the liquid. A thin-film resistor provides the heat required for vaporization. The flexing of the diaphragm wall is translated into valve movement. Thus, flow rate is governed by varying the signal voltage, for a normally open valve from 0 to 15 V. This is illustrated in Fig. 3, which shows the dynamic pressure measured at the exit of the microvalve as a function of the signal voltage. It is clear from Fig. 3 that the microvalve exhibits a nonlinear operation near the fully open and closed conditions.

Table 1 Microvalve specifications

Fluid media	Noncorrosive gases
Outlet pressure range	0–100 psig (0–6.89E5 Pa)
Maximum supply pressure	100 psig (6.89E5 Pa)
Proof/burst pressure	150/250 psig (1.03E6/1.72E6 Pa)
Flow rate range, in sccm (standard cubic centimeters per minute) (based on nitrogen at 25 psid and 25°C)	0.2–3000 sccm (4.1E-12–6.15E-8 kg/s)
Response time (0–100% full-scale rise time)	0.5 s
Average power consumption (at 50% flow capability)	0.7 W
Operating temperature range	0–40°C
Signal voltage	0–15 V
Power supply (0.250 A peak, 0.100 A continuous)	15 V

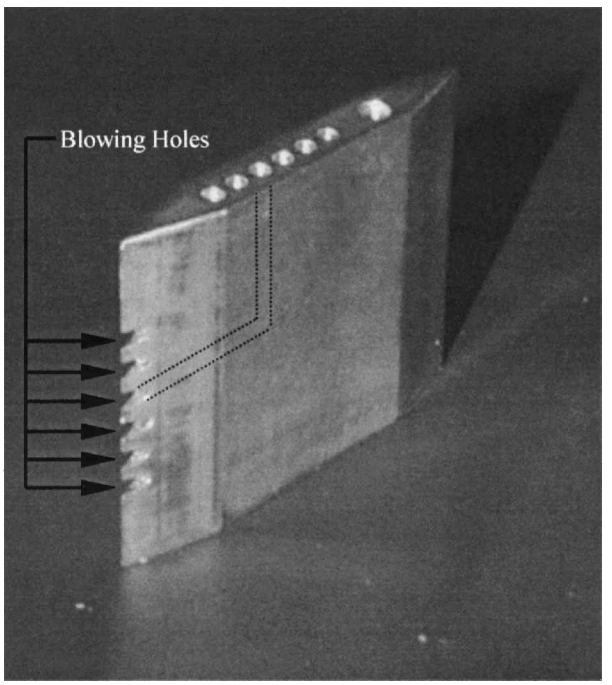

Fig. 2 Stator with trailing-edge blowing holes.

Error Sensors

The error sensors used in this study are pitot-static probes used to measure the total pressure in the wake behind each stator as

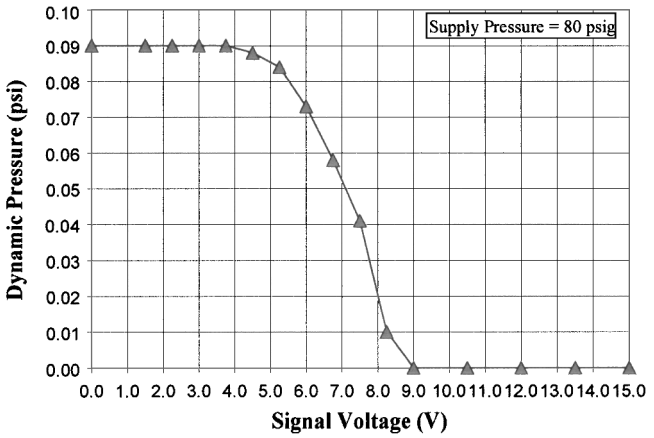

Fig. 3 Microvalve voltage response.

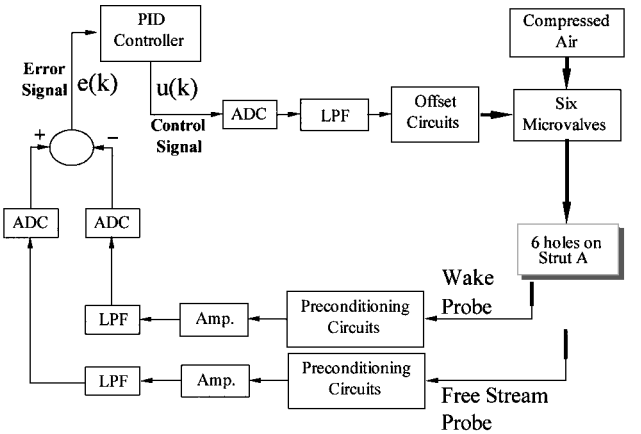

Fig. 4 Block diagram of PID controller.

shown in Fig. 1. Four threaded holes are provided in the inlet for mounting the error sensors. The holes are positioned such that each error sensor measures the maximum total pressure defect in a wake. The probes are placed $0.5C_s$ downstream of the stator, where C_s is the stator chord. This spacing was decided on after bench tests showed that a distance of $0.5C_s$ is required to allow the jet to mix into the wake. Measurements made closer to the stator will sense the potential core of the jet issuing out of the blowing hole rather than the mixed outflow and, hence, would generate an erroneous control signal. The spanwise location of the wake probes is not critical in this system because the wake is almost uniform along the stator span.[7,8] This also implies that a single wake probe is sufficient for this setup. However, for many airfoils of realistic engines the wake is not uniform, and multiple probes might be needed.

Because of their intrusive nature, it is important to remark that the use of these flow sensors may not be practical. One problem of these sensors is that they also produce a wake that is not sensed and, thus, is left unfilled. To minimize this secondary wake, the probe should be reduced in size, which could then lead to structural problem and result in durability issues. Finally, the close spacing between stators and blades typical of real engines could clearly be a limiting factor for these probes. However, active control experiments using these sensors are still very important because they provide an error signal that is directly the quantity to be minimized. Results using this flow sensing approach can then be used as an upper-limit performance curve to compare other nonintrusive sensing approaches. Note that the key goal of TEB is to improve the HCF life through the reduction of the blade strains. Thus, the optimum wake filling will yield the maximum strain reduction with the minimum blowing. Of course, fully reenergizing the wakes will lead to an improvement in the HCF life. The optimum blowing distribution is a matter of current research.

Control Algorithm

The control algorithm used in this application is a feedback proportional–integral–derivative (PID) controller. PID controllers are widely used in the process industries.[13,14] Proportional control can lead to reduced errors to disturbances but still has a small steady-state error. It can also increase the speed of response but typically at the cost of a larger transient overshoot. If the controller also includes a term proportional to the integral of the error, the error to a step can be eliminated. However, there tends to be a further deterioration of the dynamic response. Finally, addition of a term proportional to the error derivative can add damping to the dynamic response. These three terms combined form the classical PID controller.

A block diagram of the application of the PID controller to the trailing-edge blowing is shown in Fig. 4. A single-input/single-output (SISO) PID controller optimizes the blowing of each stator. The SISO controller uses the freestream pitot probe to pick up the reference signal, whereas the probe behind the stator provides the wake signal. The difference between the outputs of the two probes serves as the error signal. Each stator has six blowing holes with each hole supplied by a single microvalve. All six microvalves connected to a particular stator are driven by the same SISO controller.

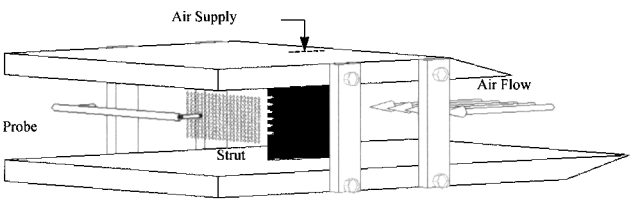

Fig. 5 Test bench.

An offset voltage is applied to ensure that the microvalves operate primarily in the linear region of the performance curve shown in Fig. 3. These offset voltages were obtained in a bench test to achieve complete filling of the wake.

Results and Discussion

In this section, the obtained results are presented and discussed. First results are presented of aerodynamic results obtained from a test bench. Results demonstrating active control are presented next, and, finally, the acoustic results are shown.

Aerodynamic Results from Test Bench

Initial aerodynamic studies were conducted with the test bench, as shown in Fig. 5. These experiments involved measuring the flowfield downstream of the stator without and with TEB. The purpose of these tests was to investigate the effectiveness of wake filling obtained by controlling individual blowing holes. This test bench was also used to determine the offset voltage for each MEMS based microvalve in the stators, as well as the supply blowing pressure. The test bench consists of two parallel Plexiglas® plates with the stator mounted in between. This assembly is placed at the exit of a blower discharge nozzle. The flowfield is measured by traversing a pitot-static probe in the grid shown. No measurements are made close to the endwalls. The trailing edge of the stator lies at the center of the traversed width. Also, the span of the traverse is restricted to the region bounding the blowing holes.

Wake Filling

The aerodynamic results are presented in the form of two-dimensional contour plots in Fig. 6. The X axis is the pitchwise direction, nondimensionalized by the stator thickness. The Y axis is the spanwise direction, nondimensionalized by the stator height. The contours display the ratio of the axial velocity to the maximum freestream velocity obtained in the measured grid. The choice of maximum freestream velocity is made to assign a common base for all ratios and also to bring out the variations that exist in the flowfield. Also seen in Fig. 6 are two vertical lines at ± 0.5 on the X axis representing the maximum thickness of the stator, with the X-axis origin locating the trailing edge. The circles with crosshairs represent the location of the TEB holes. Data are acquired $0.5C_s$ downstream of the stator, without and with blowing.

Figure 6a is a velocity ratio contour plot of the baseline case, that is, without TEB. The wake is centered about the trailing edge of the stator, as seen by the maximum velocity defect occurring at

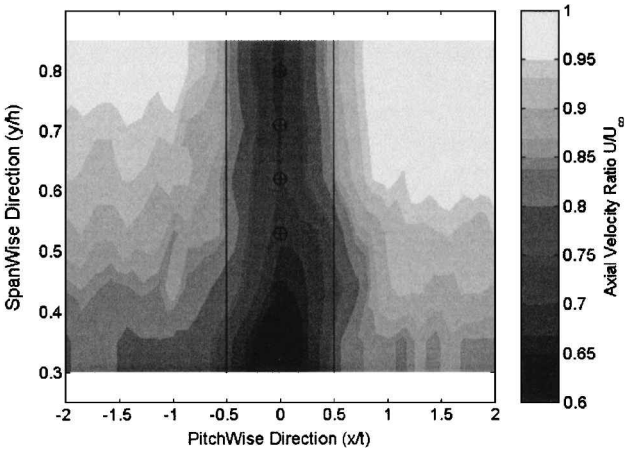

a) Without TEB

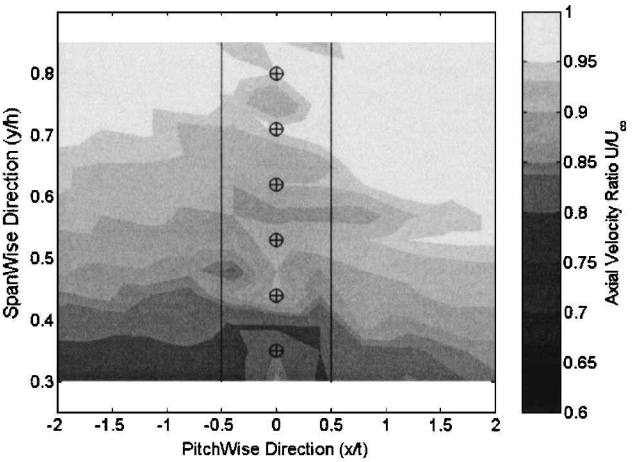

b) With TEB

Fig. 6 Comparison of axial velocity ratio.

the X-axis origin. The freestream axial velocity is not uniform in the spanwise direction, being slower closer to the hub. Figure 6b shows the velocity ratio contour plot with the application of TEB. The data are acquired after the blowing rate of each blowing hole is optimized by adjusting the voltage to the MEMS valves. The blowing rate is optimized when the total pressure in the wake equals the freestream total pressure. Two pitot-static probes are used to optimize the blowing rate. One of the probes, the reference probe, measures the freestream total pressure, which is the reference signal. The other probe, the error probe, is located behind the trailing edge of the stator and measures the maximum velocity defect generated by the stator. Both probes are located at the same streamwise distance and spanwise location downstream of the stator, with the error probe placed in line with a blowing hole. The plenum pressure is maintained constant at 85 psig (5.86×10^5 Pa). The signal voltage of the relevant MEMS microvalve is adjusted by a potentiometer, until both the probes read the same total pressure. This procedure is repeated at all six blowing hole locations, so that at each blowing hole location the total pressure behind the stator trailing edge equals the freestream total pressure at the spanwise location of the hole. The reference probe is removed and the flowfield is traversed in the pitchwise direction. By the use of this approach, the relative offset voltage to the MEMS microvalves in the stator is determined. It was found that these offset voltages were not a critical parameter.

At most spanwise locations, the wake velocity is equal to, or varies in small amount with, the axial velocity in the freestream at the same span. In addition, the spanwise variation of axial velocity in the wake is very similar to that in the freestream.

The procedure followed for optimizing the wake filling at discrete spanwise locations emphasizes the advantage of individual control in the presence of spanwise variations in the axial flow velocity in the wake region. This also helps avoid the potential of overfilling,

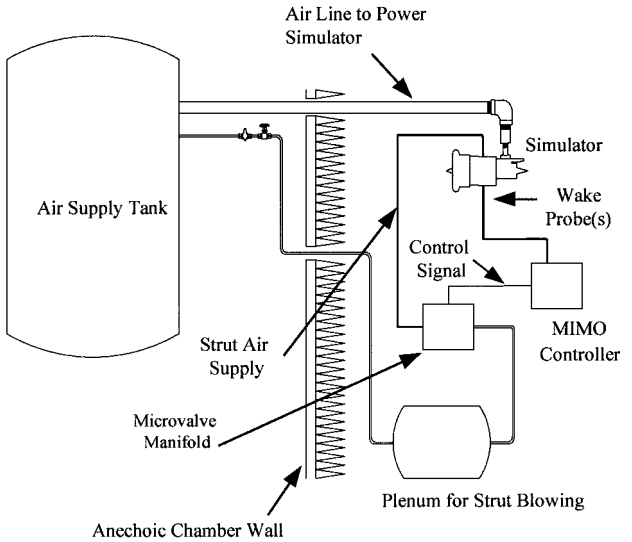

Fig. 7 Schematic of test setup.

which is as undesirable as the wake in this particular setup, where the wakes are nearly uniform along the stator span.

Setup for Active Control and Acoustic Tests

Figure 7 shows a schematic of the test setup for the active control and acoustic tests conducted in an anechoic chamber. The setup shown in Fig. 1 was mounted onto the simulator. The simulator is fixed to a support stand. High-pressure air to run the simulator is obtained from an air tank supplied by a compressor. Ducting is provided to exhaust the turbine air to the atmosphere. Air for TEB is also obtained from the same source. The air is first supplied to the plenum from which it is distributed through four pipes to the microvalve manifold. Six microvalves are connected to each of the four air lines and each microvalve in turn is connected to a single blowing hole. Before the actual tests, a preliminary investigation helped determine the following characteristics of the flowfield downstream of the stators. The maximum velocity defect is different for each stator. However, for a given stator, the axial flow velocity in the wake behind the trailing edge of the stator does not vary with radius. The freestream axial flow velocity is also uniform radially. This allowed a single error sensor to be used behind each stator, as shown in Fig. 1. Furthermore, the same control signal was applied to all microvalves on a stator.

Active Control Experiment and Results

The active flow control experimental results presented in this section were obtained on the simulator in the anechoic chamber and demonstrate the performance of the active flow control system. As mentioned earlier, the purpose of the PID feedback controller is to use the error signal to control the microvalves actively so that, as the flow condition changes in an engine, the amount of wake filling can be optimized by adjusting the microvalve.

A test was performed to demonstrate the effectiveness of the active control system to adjust to varying flow conditions. To this end, the simulator speed was changed as a function of time, and the ability of the microvalve to adjust the blowing rate to complete the wake filling was recorded. The results are shown in Fig. 8. Figure 8 shows the time histories of the control, freestream pitot probe, one of the wake pitot probes, and the simulator speed signals. The lower two traces in Fig. 8 are the pressures measured in the freestream and in one of the stator wakes. The difference between these signals is the velocity deficit or error signal to be minimized. Figure 8 clearly shows that the controller was successful in adaptively driving the microvalve so that the wake and the freestream essentially have the same velocity, thus ensuring optimal wake filling. The dynamics of the controlled system are revealed only if a drastic change in the simulator speed is produced, for example, speed changes at $t = 150$ and 200 s. For example, the simulator speed was decreased from 40,000 rpm down to 20,000 rpm in about 9 s at $t = 150$ s. From the freestream and

wake traces, the control system requires about 12 s to optimize the wake filling, that is, minimize the error signal. Similar behavior is observed at $t = 200$ s where the simulator speed is ramped up from 20,000 to 40,000 rpm. These results demonstrate that the active flow control of wakes is feasible under realistic changes in flow conditions.

Acoustic Results

Because aerodynamic measurements were not carried out, the sound field was monitored at far-field locations as an indirect indicator of the wake filling. The successful wake filling leads to the reduction of the tonal noise components due to the suppression of the interaction of the stators and the fan blades. Thus, the attenuation of the noise at the BPF and the harmonics is an indirect measurement of filling of the wake, which in turn is an indication of the reduction in blade vibration and the HCF damage. The monitored far-field microphone locations are depicted in Fig. 9. The SPL results presented in Figs. 10–12 were obtained by taking the average of 50 spectra.

Figure 10 shows the noise spectra in the far field at 20 deg of the simulator axis with and without active control. The BPF tone occurs at 8850 Hz and corresponds to a simulator speed of 29,500 rpm. These spectra demonstrate a reduction of about 8.2 dB at the BPF tone and reduction between 6 and 3 dB at the first four harmonics. The wake filling does not lead to reduction in the broadband noise component. These tonal noise reductions again clearly indicate the successful wake filling as well as the reduction of the blade forcing function and vibration. An uncertainty study was performed to determine the confidence in the experimental results. The mean power and standard deviation for the BPF and 2BPF tones were computed without and with active flow control. The confidence interval was computed using these values, and they are presented in Table 2.

The radiating directivities at the BPF were also obtained for the purpose of estimating the SPL. The confidence interval, that is, mean plus or minus standard deviation, is also shown in Figs. 11 and 12 as dotted. Figure 11 compares the directivity of the BPF tone at 29,500 rpm without and with TEB. As observed, the BPF tone is reduced at all recorded positions except at 0 deg, which lines up with the axis of the simulator. Significant reductions, greater than 3 dB, are obtained at most positions. The maximum reduction is 8.2 dB at the 20-deg position, which agrees well with the 7-dB reduction obtained in the work by Leitch [7] and Leitch et al.[8] Note that aerodynamic measurements by Leitch[7] and Leitch et al.[8] showed nearly full filling of the wake in their experiments. Because the same setup is used, it is quite reasonable to conclude that nearly complete filling of the wake is also achieved here.

Figure 12 compares the directivity of the BPF tone at 40,000 rpm without and with TEB. The BPF tone shows reduction in the sector from 0 to 40 deg. The maximum reduction obtained is 7.3 dB at 20 deg. In the sector from 60 to 110 deg, it can be observed that the SPL remains the same, with and without TEB.

TEB to reenergize the wakes from the stators results in the suppression of the stator–rotor interaction effect. However, the far-field radiation is due to the contribution of several noise sources, in particular the stator–rotor and the rotor–EGV interactions. Thus, the maximum allowed reduction in the radiation directivity from reenergizing the stator wakes is limited by the presence of the rotor–EGV interaction. In the experiments performed to obtain the radiation directivities, the wakes were effectively reenergized, that is, the wake total pressure was equal to the freestream total pressure (see Fig. 8). Because of this, it is believed that the radiation directivities with TEB shown in Figs. 11 and 12 are mainly due to the rotor–EGV interaction.

The radiated sound power was computed from the radiation directivities by integrating the far-field acoustic intensity. Determining the sound power has the advantage that it describes the sound energy output of the source, without regard to the directivity. This provides a more direct understanding of the effect of TEB on source strength. Because the resolution of the recorded data is not high, this analysis provides an estimate of the sound power level, and the change in sound power level with TEB helps us to better understand the effect trailing edge blowing has on the unsteady interaction.

The BPF power reduction is significant at both test speeds. At 29,500 rpm, the power in the BPF tone was reduced by 4.4 dB. At 40,000 rpm, the reduction in the BPF tone power was 2.9 dB. A reduction in far-field acoustic power can be directly interpreted as a reduction of similar magnitude in the source power. TEB reduces the magnitude of the velocity defect seen by the rotor and

Table 2 Confidence interval analysis at 20 deg

Parameter, μ = mean, σ = standard deviation	BPF tone, dB		2BPF tone, dB	
	Without TEB	With TEB	Without TEB	With TEB
$\mu + \sigma$	95.2	87.1	94.0	88.0
μ	94.8	86.6	93.7	87.6
$\mu - \sigma$	94.3	85.9	93.3	87.1

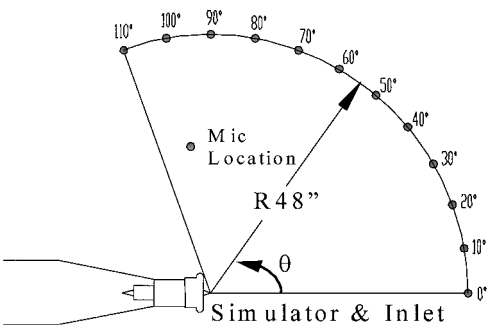

Fig. 9 Position of far-field monitoring microphones.

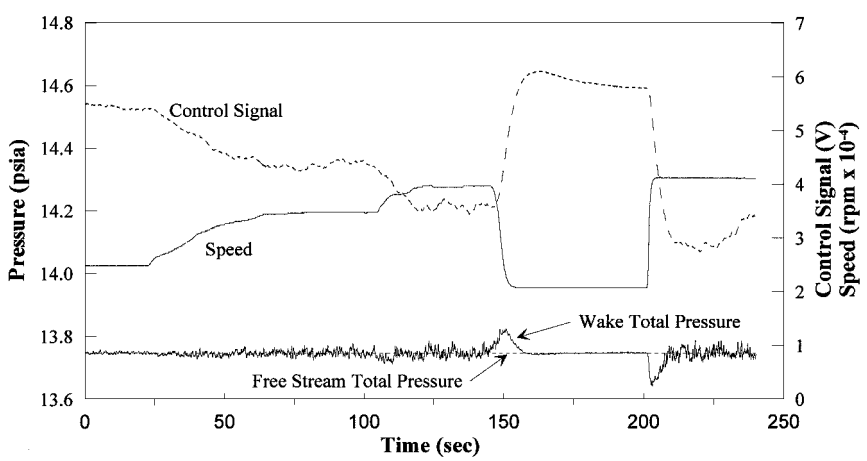

Fig. 8 Time histories of control, pressure pitot probes, and simulator speed signals.

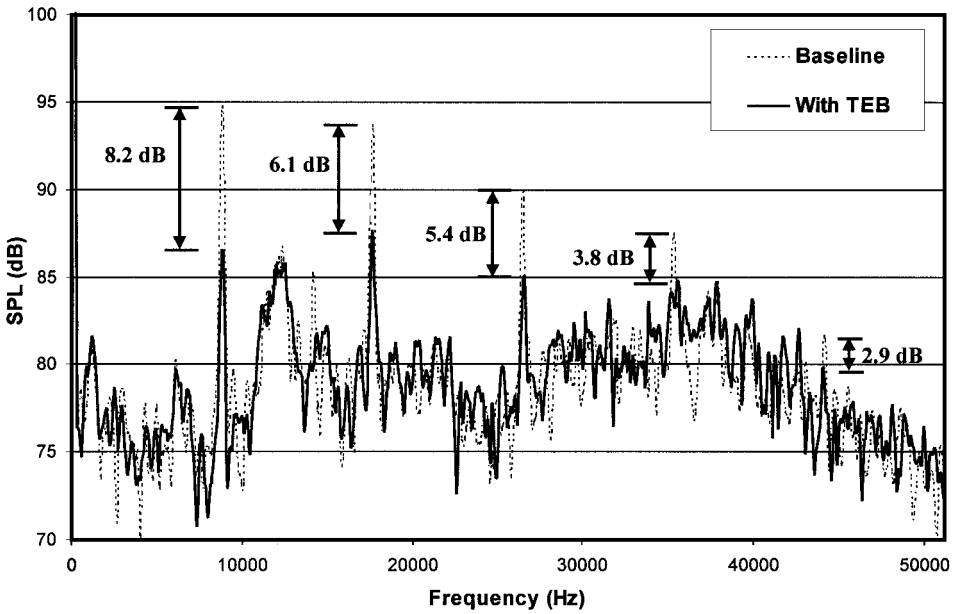

Fig. 10 Far-field acoustic spectrum at 20 deg without and with active flow control.

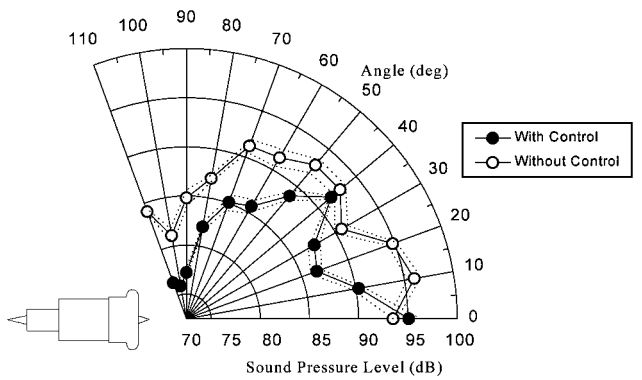

Fig. 11 Directivity of BPF tone at 29,500 rpm, confidence interval (· · ·).

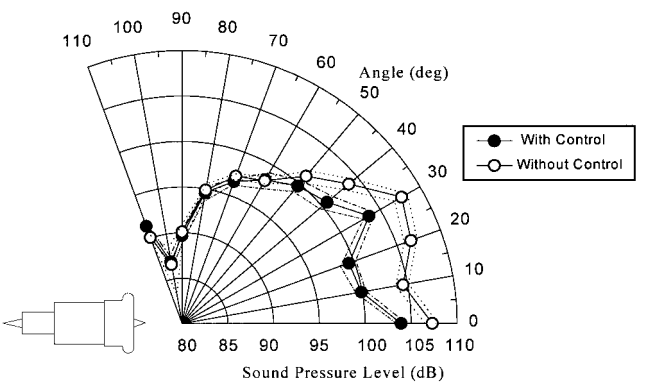

Fig. 12 Directivity of BPF tone at 40,000 rpm, confidence interval (· · ·).

also smoothes the velocity profile. Furthermore, this decreases the unsteady loading experienced by the blade as it passes through the wake and, hence, the reduction in source strength. The lesser power reduction at the higher speed is probably because with an increase in speed the acoustic power generated by the rotor and the EGVs interaction increases.

Conclusions

An active flow control system is developed to obtain effective wake management through TEB in a rotating environment. The flowfield downstream of a stator row is characterized by the presence of wakes. These are discrete flow regions where the axial flow velocity is lower than that in the freestream. Furthermore, the velocity profile varies throughout the wake region. When a rotor chops through the wakes, it experiences unsteady loading due to continuous variation in the inlet flow velocity. This causes blade vibration and the associated strain cycles that lead to HCF damage. In addition, the unsteady stator–rotor interaction results in acoustic energy at discrete frequencies, that is, BPF tone and harmonics. To reduce or eliminate these effects of unsteady interaction, the wake is reenergized by injecting mass from the trailing edge of the stator vanes.

In this investigation, a symmetric inlet with four upstream support stators is mounted on a turbofan simulator. These stators generate four wakes, and the periodic interaction of the rotor blades with these velocity defects generates discrete frequency noise. The experiment is set up in an anechoic chamber, and the discrete frequency noise is measured by placing microphones in the far field. Next, the wakes are reenergized by TEB. To this end, each stator is provided with six discrete holes spaced equally along the stator span. The air supply to each blowing hole is controlled by individual MEMS based microvalves. A four-channel PID controller generates the signal voltage that controls the flow rate through each microvalve. The inputs to the PID controller are the total pressures in the freestream and wakes behind each stator. The error signal is computed as the difference between these signals, with the freestream total pressure as the reference. Pitot probes immersed in the flow measure the wake total pressures that are used as inputs to the controller. Thus, an active flow control system is incorporated. The advantages of this system are that effective wake filling is achieved and that changes in operating condition can be tracked for effective wake management with changing conditions.

From the results presented, it can be concluded that controlling the blowing rate of each hole produces a very uniform flowfield downstream of the stator. In addition to eliminating or reducing the circumferential variations, the radial gradient present in the freestream flow is maintained in the wake region after effective filling is achieved. The ability of the system to achieve effective wake filling when subjected to a change in inlet flow conditions demonstrates the feasibility and advantage of active flow control. It was also demonstrated that far-field SPLs at the relevant discrete frequencies are reduced by TEB. Furthermore, the reduction in source strength caused by eliminating or decreasing the circumferential velocity defects supports the effectiveness of TEB in reducing unsteady stator–rotor interaction. The maximum sound level reduction is observed at the blade passing frequency of each tested speed. The maximum tone reductions obtained are 8.2 dB at 29,500 rpm and

7.3 dB at 40,000 rpm. Sound power level at the BPF tone, calculated from the measured directivity, is reduced by 4.4 dB at 29,500 rpm and 2.9 dB at 40,000 rpm.

Acknowledgments

This work is supported by the Air Force Office of Scientific Research and NASA John H. Glenn Research Center at Lewis Field. Partial support is also provided by the Department of Mechanical Engineering at Virginia Polytechnic Institute and State University. The authors are indebted to Oral Mehmed and Carl Lorenzo for many useful discussions. The authors also gratefully acknowledge the contributions of Shiming Li, William Stinnett, Thomas Leitch, David Harper, Oliver Popp, and Todd Bailie.

References

[1]Goldstein, M. E., "Aeroacoustics," NASA SP-346, Jan. 1974.

[2]Pande, A., and Ng, W. F., "Effect of Stators on the Aeroacoustics of Axisymmetric Supersonic Inlets: Part 1—Experimental Results," AIAA Paper 95-2887, July 1995.

[3]Waitz, I. A., Brookfield, J. M., Sell, J., and Hayden, B. J., "Preliminary Assessment of Wake Management Strategies for Reduction of Turbomachinery Fan Noise," *Journal of Propulsion and Power*, Vol. 12, No. 5, 1996, pp. 958–966.

[4]Naumann, R. G., "Control of the Wake from a Simulated Blade by Trailing Edge Blowing," M.S. Thesis, Dept. of Mechanical Engineering, Lehigh Univ., Bethlehem, PA, July 1992.

[5]Corcoran, T. E., "Control of the Wake from a Simulated Blade by Trailing Edge Blowing," M.S. Thesis, Dept. of Mechanical Engineering, Lehigh Univ., Bethlehem, PA, Jan. 1992.

[6]Park, W. J., and Cimbala, J. M., "The Effect of Jet Injection Geometry on Two-Dimensional Momentumless Wakes," *Journal of Fluid Mechanics*, Vol. 224, 1991, pp. 29–47.

[7]Leitch, T., "Reduction of Unsteady Stator–Rotor Interaction by Trailing Edge Blowing," M.S. Thesis, Dept. of Mechanical Engineering, Virginia Polytechnic Inst. and State Univ., Blacksburg, VA, Jan. 1997.

[8]Leitch, T., Saunders, C. A., and Ng, W. F., "Reduction of Unsteady Stator–Rotor Interaction Using Trailing Edge Blowing," AIAA Paper 99-1952, May 1999.

[9]Saunders, C. A., "Noise Reduction in an Axisymmetric Supersonic Inlet Using Trailing Edge Blowing," M.S. Thesis, Dept. of Mechanical Engineering, Virginia Polytechnic Inst. and State Univ., Blacksburg, VA, Jan. 1998.

[10]Brookfield, J. M., and Waitz, I. A., "Trailing-Edge Blowing for Reduction of Turbomachinery Fan Noise," *Journal of Propulsion and Power*, Vol. 16, No. 1, 2000, pp. 57–64.

[11]*Technical Data/Design Specifications*, Redwood Microsystems, Inc., Menlo Park, CA, 1997.

[12]*Operating Principles–Fluistor Microvalve*, Redwood Microsystems, Inc., Menlo Park, CA, URL: http://www.redwoodmicro.com/principles.html, Aug. 1998.

[13]Franklin, G. F., Powell, J. D., and Workman, M. L., *Digital Control of Dynamic Systems*, Addison Wesley Longman, Reading, MA, 1997, pp. 21–50.

[14]Phillips, C. L., and Harbor, R. D., *Feedback Control Systems*, Prentice–Hall, Upper Saddle River, NJ, 1996, pp. 537–586.

M. Samimy
Associate Editor